LA-UR-19-26162
Approved for public release; distribution is unlimited.

Title: Verification test of the SURF model in xRage: Part IV cylindrically converging detonation wave

Author(s): Menikoff, Ralph

Intended for: Report

Issued: 2019-06-28

Verification test of the SURF model in xRage: Part IV Cylindrically Converging Detonation Wave

Ralph Menikoff

June 24, 2019

Abstract

Previous verification studies of the SURF reactive burn model in the xRage code used test problems for underdriven or self-supporting detonation waves. Here we consider overdriven detonation waves. As a test problem we use a cylindrical converging detonation wave. Since there is no exact solution, the numerical solutions at different resolutions are compared for 1-D cylindrical geometry and 2-D Cartesian geometry.

1 Introduction

SURF is a high explosive (HE) reactive burn model for shock initiation and propagation of detonation waves. It is based on the ignition and growth concept of hot spots [Menikoff and Shaw, 2010] and features a burn rate that is a function of the lead shock pressure along with an algorithm to detect the lead shock based on the Hugoniot energy equation [Menikoff, 2016a]. The SURF model has been implemented in the Eulerian xRage code with adaptive mesh refinement (AMR). The AMR capability is used to increase the resolution in the reaction zone of a detonation wave.

Previous verification tests of the xRage implementation of SURF examined a propagating underdriven detonation wave in 1-D (for which there is an exact solution) [Menikoff, 2016b,c]. In addition, as a test of the shock detector and for numerical mesh alignment effects, a 2-D simulation in Cartesian geometry of a cylindrically diverging detonation wave was compared with a high resolution 1-D simulation in cylindrical geometry [Menikoff, 2016d].

Here the verification tests are extended to include the propagation of overdriven detonation waves. As a test problem we use a cylindrically converging detonation wave. A converging detonation has a quasi-steady reaction-zone profile. The wave strengthens and speeds up due to a geometric source term (last term on right hand side) in the forward (direction of wave propagation) characteristic equation

$$[\partial_t + (u-c)\partial_r]P - \rho c\,[\partial_t + (u-c)\partial_r]u = (\partial_\lambda P)_{V,e}\,\mathcal{R}ate - \rho c^2 u\kappa \;, \tag{1}$$

where the front curvature is $\kappa = -1/r$ for a cylindrically converging wave. Consequently, a converging detonation samples an interval on the strong branch of the detonation locus. We note that the geometric source term also shifts the detonation locus up in the (V, P) plane, which gives a slightly higher detonation speed for a given detonation pressure.

In contrast to the propagation of a planar detonation wave, there is no exact or semi-analytic solution for diverging or converging detonation waves. As with the diverging case, for the converging detonation we study the effect of mesh resolution for 1-D simulations in cylindrical geometry. In addition, we compared a 2-D simulation in Cartesian geometry with a 1-D simulation in cylindrical geometry to check for numerical mesh alignment effects.

2 Simulations

The simulations use a reactive burn model for PBX 9501. The HE model and the setup for the simulations are described next.

2.1 HE model

A reactive burn model consist of two parts. Equations of state (EOS) for the reactants and products with PT equilibrium for partly burned HE, and the burn rate. For PBX 9501 we use the Davis EOS for the reactants and products. The fitting form is described in [Aslam, 2018, App. A and B] and the xRage input parameters are given in Appendix A. Unlike many other EOS models, we note that the reactant shock locus and the products detonation locus, shown in fig. 1, do not cross. As the detonation pressure increases, the chemical energy release becomes less important relative to the shock energy, and the von Neumann (VN) spike (lead shock) pressure approaches the detonation pressure at the end of the reaction zone. This is shown in fig. 2 along with the overdrive; *i.e.*, the excess of the characteristic speed over the detonation speed.

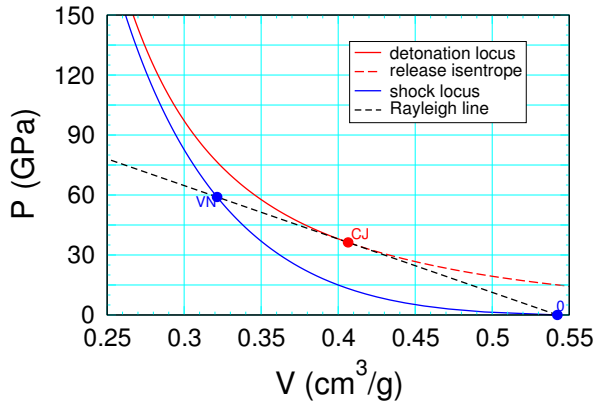

Figure 1: Shock and detonation loci for PBX 9501 with the Davis EOS.

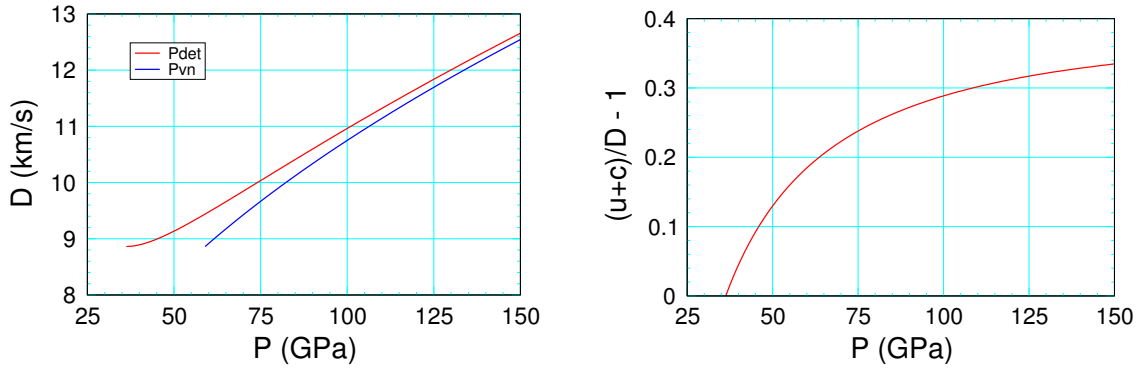

Figure 2: Detonation speed and overdrive on the strong branch of the detonation locus.

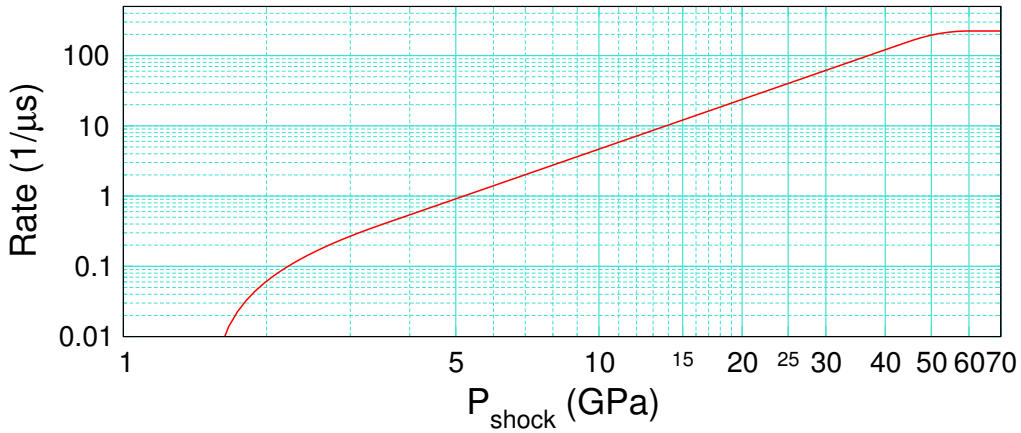

Figure 3: SURF burn rate for PBX 9501.

The fitting form for the SURF rate is described in [Menikoff, 2017, App. A] and the xRage input parameters are given in Appendix B. The rate as a function of shock pressure is plotted in fig. 3. We note that the SURF rate is motivated by the concept of hot spots and saturates at a shock pressure of 60 GPa (slightly above the VN spike pressure of a CJ detonation wave) with a rate of $224/\mu$s. For strongly overdriven detonation waves, the shock temperature is high enough that the bulk chemical rate would substantially contribute to the burn rate. In principle an Arrhenius term can be added to the hot-spot rate. This is somewhat problematic as the thermal component of most reactants EOS models are not accurate and the resolution requirement for a much higher rate would be computationally expensive.

2.2 Setup

The initial configuration of the simulation consists of a 40 mm cylinder of PBX 9501 surrounded by a 4 mm thick annulus of steel and then air. The steel is given a radial inward velocity with a gradient; 1.5 km/s at the inner surface and 0 at the outer surface. The velocity gradient minimizes a startup transient at the steel/air interface. The steel drives a 11.6 GPa shock into the PBX and promptly initiates (within 2 mm) a converging detonation wave.

After traveling about 1 mm, the inward motion of the inner steel surface is arrested by the pressure behind the detonation wave. Consequently, other then initiating the detonation, the steel has little influence on the detonation front. The simulations are stopped when the detonation front reaches a radius of 1 mm. This avoids the singularity at the origin but still gives a large ratio for the initial to final radii of the detonation front.

Adaptive mesh refinement is used to better resolve the reaction zone of the detonation wave. In 1-D cylindrical geometry three simulations were run with fine, standard and coarse reaction-zone cell size of 2, 7.8 and 32 μm, respectively. To check on mesh alignment effects, a 2-D Cartesian geometry simulation was run. Due to the increased computational cost, the 2-D simulation used a reaction-zone cell size of 15.6 μm. The 2-D simulation was compared with a 1-D simulation at the same resolution. This simplifies the comparison since it minimizes the variation of the detonation front position due to numerical resolution.

3 Numerical results

3.1 1-D cylindrical geometry

A sequence of pressure profiles as the detonation wave converges is shown in fig. 4. Aside from the VN spike, the resolution has only a small effect on the profiles until small radii when the detonation pressure becomes very large (about 3 times the CJ pressure). The lead shock pressure and the detonation speed are shown in fig. 5. These quantities are obtained from the shock detector used by the SURF model. The shock pressure is averaged over 4 time steps to reduce high frequency noise. For a smoother detonation speed an average is taken over 0.1 mm (approximately the reaction-zone width) for the standard and fine resolution and over 0.2 mm for the coarse resolution. We note that the numerical noise in the detonation speed is greatly reduced at the finer resolution.

There are 2 general trends with resolution. First, the shock pressure is lower at coarse resolution because the VN spike is clipped. This is seen clearly in the reaction-zone profiles shown in fig. 6. Second, the detonation speed changes slowly at first and then rapidly accelerates after the front reaches half the initial radius.

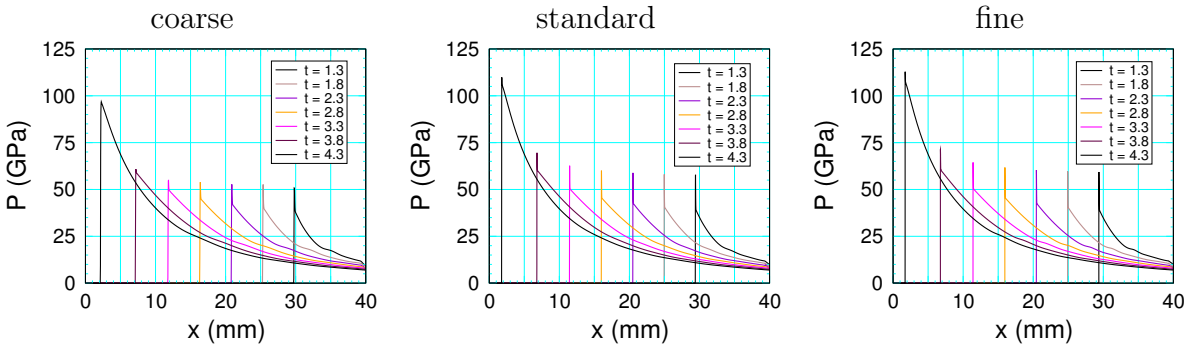

Figure 4: Sequence of pressure profiles for simulations at three resolutions.

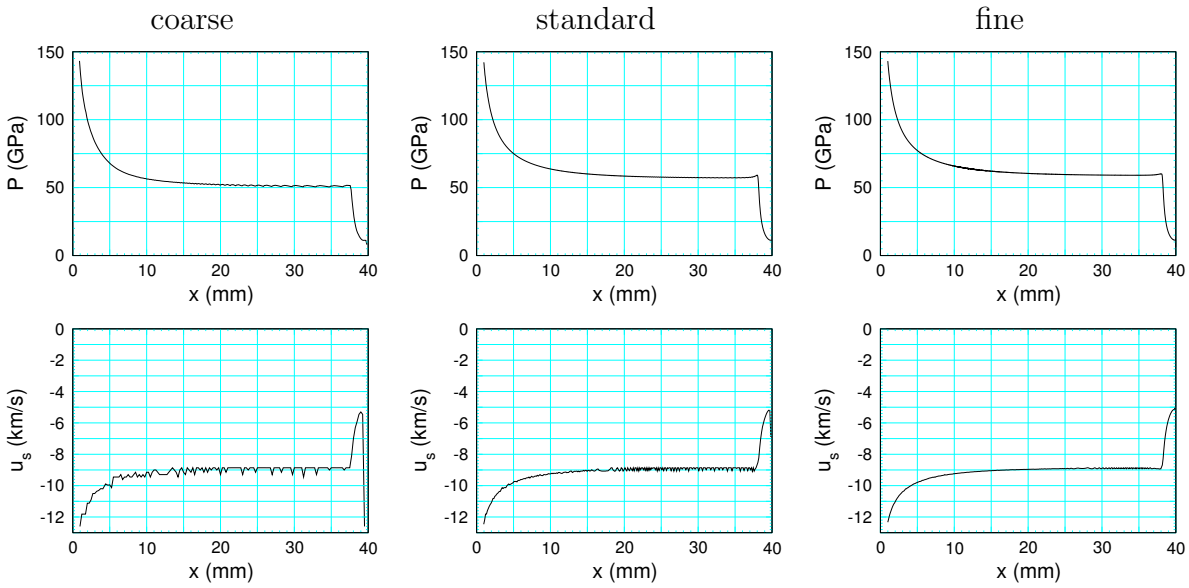

Figure 5: Lead shock pressure and detonation velocity vs radius from the SURF shock detector for simulations at three resolutions.

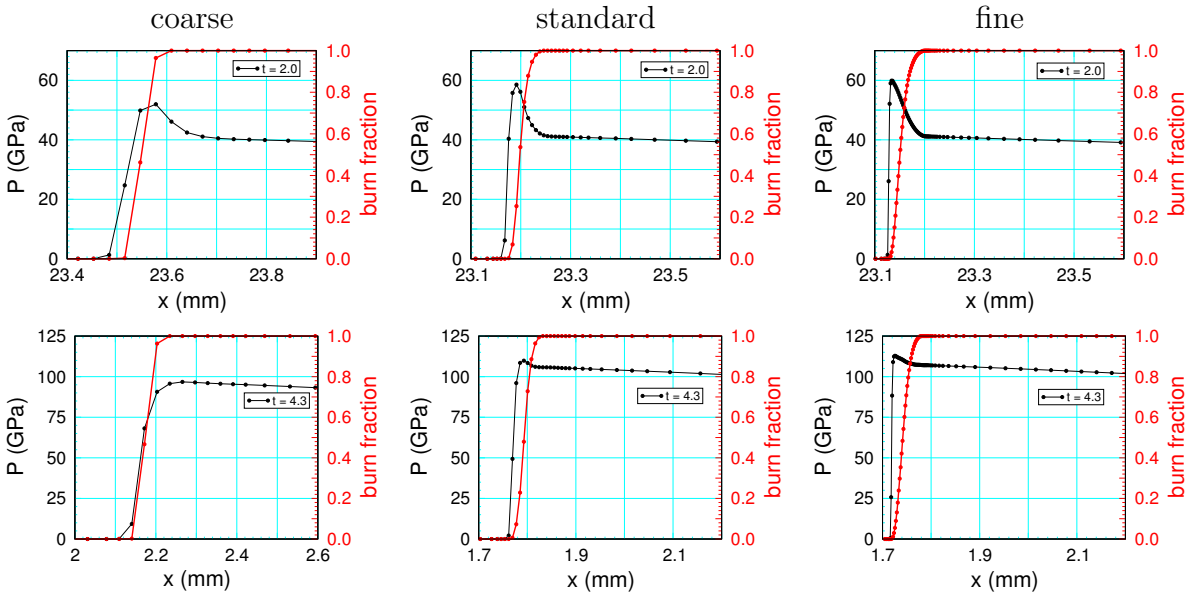

Figure 6: Pressure profiles in the neighborhood of the reaction zone for simulations at three resolutions. Top plots correspond to time when detonation front is at about half its initial radius. Bottom plots are near end of run when detonation front has undergone a large radial convergence.

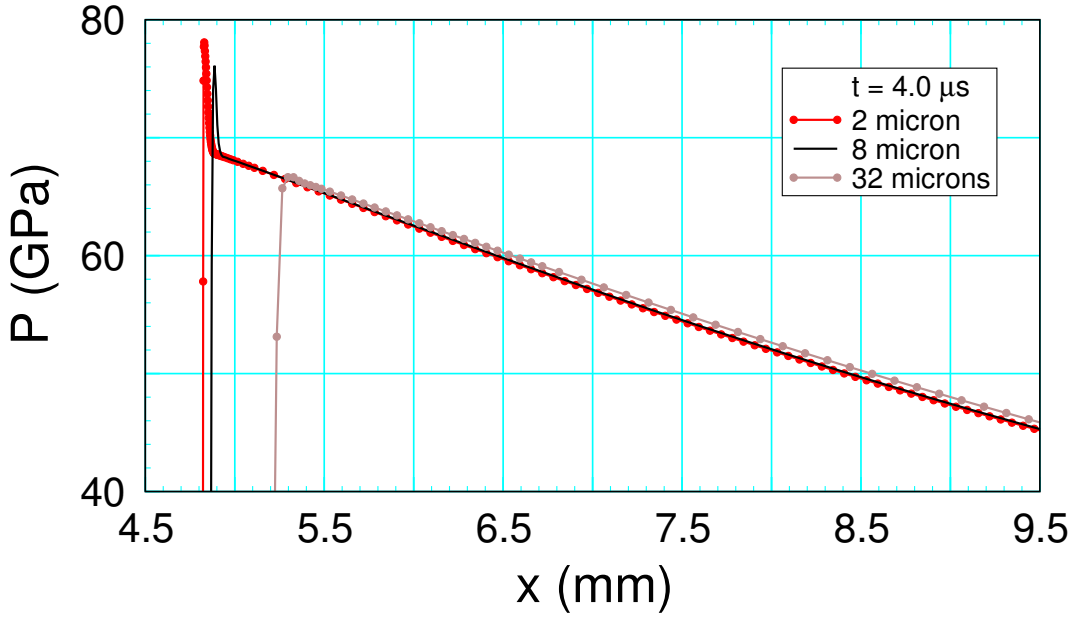

Figure 7: Comparison of pressure profiles at $t = 4\,\mu$s for the fine, std and coarse resolution simulations.

It can be seen from the reaction-zone profiles displayed in fig. 6 that the number of cells in the reaction zone varies; about 2, 6 and 24 for the coarse, standard and fine resolutions, respectively. At the coarse resolution there is significant reaction in the shock rise. The fine resolution shows the effect of the von Neumann spike pressure getting closer to the detonation pressure for stronger overdriven detonations as shown in fig. 2.

A comparison with resolution of pressure profiles near the end of the simulations is shown in fig. 7. The profiles for the fine and std resolution simulations are quite close. This indicates that the fine resolution solution is near mesh converged. The detonation front for the coarse resolution is behind by 0.3 to 0.4 mm out of a run distance of 35 mm due to the cumulative effect of a slightly lower detonation speed. In addition, the release wave has a slightly lower slope. Overall the profile for the coarse resolution simulation, despite not resolving the reaction zone, is fairly close to the resolved solution.

Two additional fine resolution simulations were run with smaller and larger HE radii, 30 and 50 mm, respectively. The shock pressure and shock speed are shown in fig. 8 for the three HE lengths. With the radial coordinate scaled such that the initiation position of the detonation wave coincide, the curves nearly lie on top of each other. We note that the scaling can not be exact since the dimensional parameters of the model prevent a similarity solution from existing. Nevertheless, within a range of HE lengths the scaling does remarkable well.

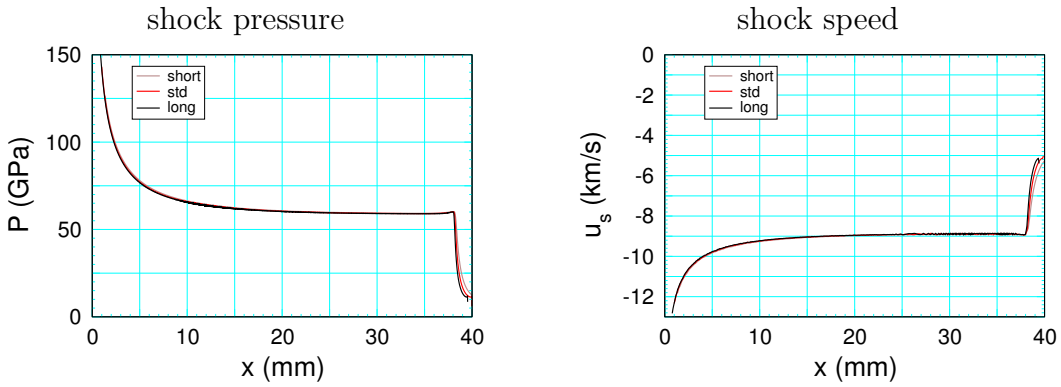

Figure 8: Shock pressure and shock speed for three HE lengths. The x-coordinate for the short and long HE simulations have been scaled such that the initiation position of the detonation wave coincides with that of the standard case (38 mm).

3.2 2-D cylindrical geometry

A 2-D simulation in Cartesian geometry was run to test whether xRage would maintain the cylindrical symmetry. The worst case for symmetry is at the end of the simulation. Figure 9 shows a 2-D pressure plot when the detonation front reached a radius of 1.8 mm. Grid lines

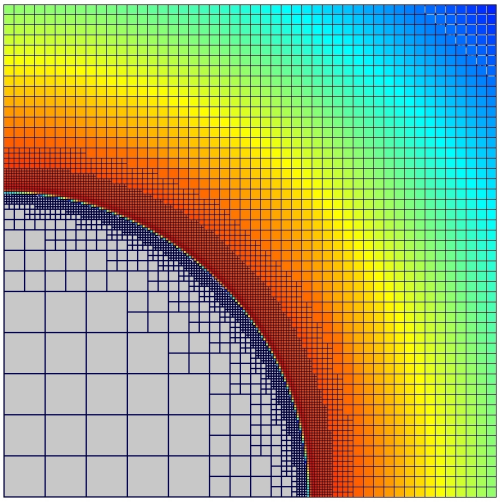

Figure 9: 2-D pressure plot near end of run; $t = 4.3\,\mu$s when front is at $r = 1.8$ mm. Pressure ranges from 70 (blue) to 110 (red) GPa, and gray for 1 bar ahead of the detonation. Plot is zoomed in on 3 mm neighborhood of the origin (lower left corner). Grid lines in black show the adaptive mesh grid.

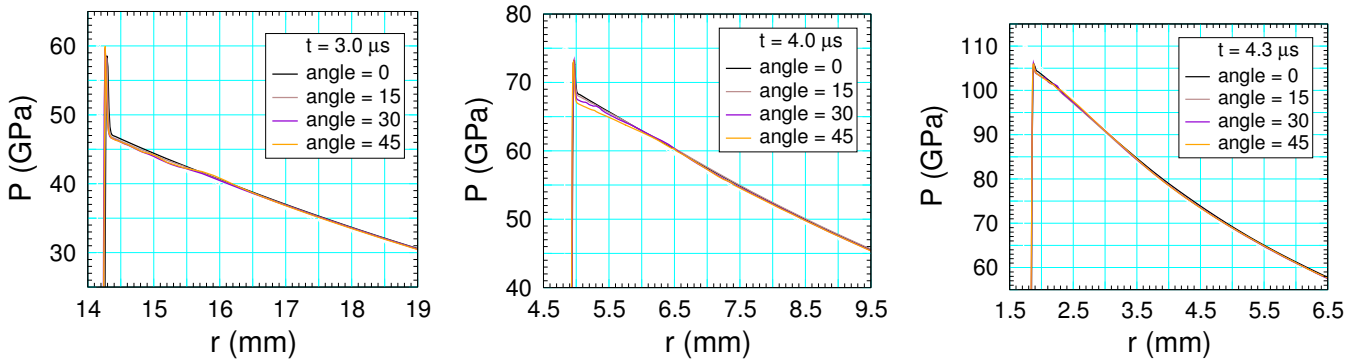

Figure 10: Pressure profile along rays at selected times.

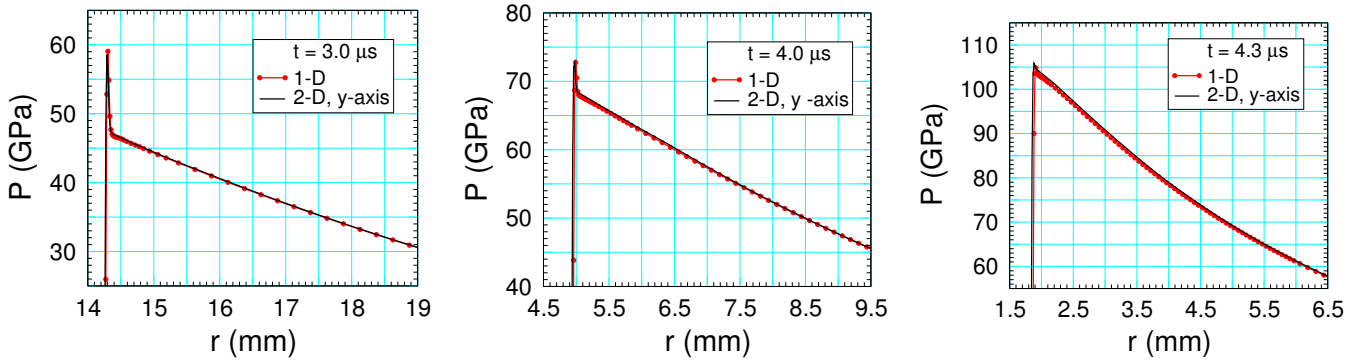

Figure 11: Comparison of pressure profiles for 1-D simulation and 2-D simulation along y-axis at selected times.

superimposed on the pressure field show the mesh adapting from a cell size of 0.25 mm for the level 1 grid in the ambient state to 0.015 mm for the level 5 grid in the reaction zone behind the detonation front. By eye the cylindrical symmetry is good.

A more quantitative measure of the symmetry is the comparison of the pressure profile along rays shown in fig. 10. There is slight variation with angle for a 0.5 mm behind the detonation front. After that the profiles along the rays nearly lie on top of each other. A comparison of the 2-D profile along the y-axis and the 1-D profile is shown in Figure 11. The same resolution is used for both simulations to minimize the difference in the positions of the shock front. It is seen that the profiles for the 1-D and 2-D simulations nearly lie on top of one another.

A sequence of pressure profiles along the y-axis is shown in fig. 12. Superimposed on the plot is the profile of the lead shock pressure grid variable determined by the SURF model shock

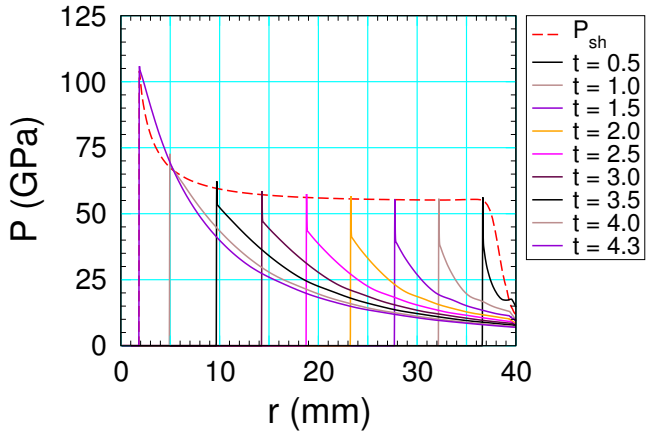

Figure 12: Pressure profiles along y-axis at sequence of times with the advected shock pressure superimposed.

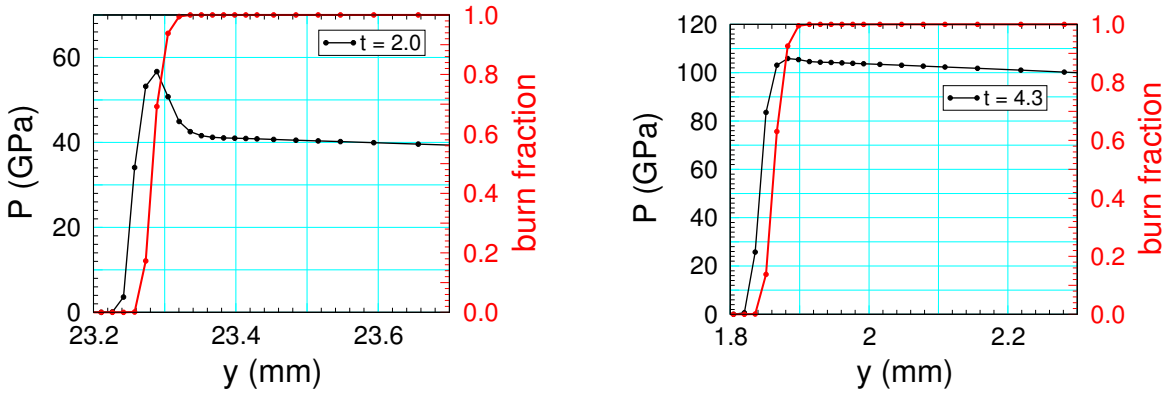

Figure 13: Profiles in the neighborhood of reaction zone at 2 and 4 μs.

detector. The shock pressure profile should go through the peak of each pressure profile. It is a little low since the shock pressure is an advected variable and the lead shock pressure increases with time. Thus the advected shock pressure profile at late time is slightly lower than the peak pressure for profiles at an earlier time.

Pressure profiles in the neighborhood of the detonation front are shown in fig. 13. The profiles at 2 μs and 4.3 μs, have a resolution between that of the coarse and standard 1-D profiles shown in fig. 6. Also the front positions are between that of the 1-D coarse and standard resolutions. This is as expected from the relative cell size used for each of the simulations.

4 Summary

The simulations of a converging detonation show that the wave accelerates slowly when the front radius decreases by a factor of 2; from 40 to 20 mm. The acceleration increases rapidly when the front radius is below 10 mm. To resolve the reaction zone requires a cell size of 2 μm. With lower resolution the von Neumann spike pressure gets clipped and there is substantial reaction in the lead shock rise. Nevertheless, the effect on the shock pressure and shock speed is relatively small. Though there is a cumulative effect on the front trajectory as time and run distance increase.

Comparisons between SURF simulations with a 1-D cylindrical mesh and 2-D Cartesian mesh show good agreement with only small 2-D asymmetry at late time. The SURF model uses a burn rate motivated by the concept of hot spots. The rate saturates around the von Neumann spike pressure for a CJ detonation. Physically, one expects the chemical rate at the shock temperature to dominate for sufficiently strong overdriven detonations that occur at large convergence ratios. The higher rate would require higher resolution for the reaction zone. However, the chemical energy released by the reaction becomes small relative to the lead shock energy as the overdrive increases. Very likely using a higher rate and better resolving the reaction zone of strongly overdriven detonation waves would not significantly increase the accuracy of a converging detonation wave simulation.

Finally, we note that the 2-D simulation with a reaction-zone cell size of 15.6 microns used about 2 million cells and took 8.4 hours on 72 processors. By comparison the 1-D simulation with the standard reaction-zone cell size of 7.8 microns had only 1000 cells and took 6 minutes on 1 processor. Thus, even with AMR, better resolving the reaction zone in 2-D and more so in 3-D would be computationally very expensive. An important question is whether the increase in accuracy warrants the expense.

References

T. D. Aslam. Temperature dependent rate law for plastic bonded explosives. *J. Appl. Phys.*, 123:145901, 2018. URL https://doi.org/10.1063/1.5020172. 3

R. Menikoff. Shock detector for SURF model. Technical Report LA-UR-16-20116, Los Alamos National Lab., 2016a. URL http://www.osti.gov/scitech/servlets/purl/1234496. 2

R. Menikoff. Verification test of the SURF and SURFplus models in xRage. Technical Report LA-UR-16-23636, Los Alamos National Lab., 2016b. URL https://www.osti.gov/scitech/servlets/purl/1254247. 2

R. Menikoff. Verification test of the SURF and SURFplus models in xRage: Part II. Technical Report LA-UR-16-24352, Los Alamos National Lab., 2016c. URL https://www.osti.gov/scitech/servlets/purl/1258358. 2

R. Menikoff. Verification test of the SURF and SURFplus models in xRage: Part III affect of mesh alignment. Technical Report LA-UR-16-26317, Los Alamos National Lab., 2016d. URL https://www.osti.gov/scitech/servlets/purl/1304803. 2

R. Menikoff. SURFplus model calibration for PBX 9502. Technical Report LA-UR-17-31015, Los Alamos National Lab., 2017. URL https://doi.org/10.2172/1412839. 4

R. Menikoff and M. S. Shaw. Reactive burn models and Ignition & Growth concept. *EPJ Web of Conferences*, 10, 2010. doi: 10.1051/epjconf/20101000003. URL http://www.epj-conferences.org/articles/epjconf/pdf/2010/09/epjconf_nmh2010_00003.pdf. 2

Appendix A. EOS parameters

```
! ---- 9501 Davis reactants
!      density 1.844 g/cm^3
matid(1)     = 919501         ! table number
matident(1)  = 'PBX9501-reactant'
eostype(1)   = 14             ! Davis reactants EOS
matdef( 2,1) = 1e10           ! Pscale, 1GPa
matdef( 3,1) = 1.844          ! rho0
matdef( 4,1) = 0.0            ! e0
matdef( 5,1) = 1e-4           ! P0
matdef( 6,1) = 300            ! T0, K
matdef( 7,1) = 2.339          ! A, km/s
matdef( 8,1) = 2.737          ! B
matdef( 9,1) = 1.45           ! C
matdef(10,1) = 0.7989         ! Gamma0
matdef(11,1) = -0.03076       ! Z
matdef(12,1) = 1.088e-3       ! alpha (table VI)
matdef(13,1) = 0.979e-3       ! Cv, MJ/kg/K
!
! ---- 9501 Davis products
matid(2)     = 929501         ! table number
matident(2)  = 'PBX9501-products'
eostype(2)   = 15             ! Davis products EOS
matdef( 2,2) = 1e10           ! Pscale, 1GPa
matdef( 3,2) = 1.844          ! rho0
matdef( 4,2) = 0.0            ! e0
matdef( 5,2) = 0.0            ! P0
matdef( 6,2) = 0.8314         ! Vc
matdef( 7,2) = 3.738          ! Pc
matdef( 8,2) = 2407.34        ! Tc, replace with default

matdef( 9,2) = 0.7965         ! a
matdef(10,2) = 0.70           ! b
matdef(11,2) = 1.758          ! n
matdef(12,2) = 1.3            ! k
matdef(13,2) = 0.945e-3       ! Cv, MJ/kg/K
```

Appendix B. SURF PBX 9501 parameters

```
he_model(1)     = 6                 ! SURF
he_unreacted(1) = 1                 ! reactants
he_reacted(1)   = 2                 ! products
he_specific_energy(1) = $Edet       ! extra energy release
he_SURF_Pburn   = (35*$GPa)
!
he_zone_size(1)   = (0.007*$mm)     ! refine to zone_size
he_dtpct          = 0.25            ! cfl parameter for HE
he_w_cutoff(1)    = 0               ! burn fraction cutoff
he_refine_dw(1)   = 0.0001          ! dw for refinement
!
he_pscale(1)    = (1*$GPa)          ! pressure unit for rate
he_tscale(1)    = (1*$microsec)     !     time unit for rate
!
! ds/dt = f(Ps)*(P/Ps)**n
! Fitting form 4
!
he_surf_P0(1)    =  1.5               ! units of pscale
he_surf_Plow(1)  =  3.5               ! units of pscale
he_surf_P1(1)    = 45.0               ! units of pscale
he_surf_Phigh(1) = 60.0               ! limit rate at Phigh, units of pscale

he_surf_C(1)     = 0.020802           ! units 1/tscale
he_surf_fn(1)    = 2.35

he_surf_n(1)     =  1.0
he_surf_nhi(1)   =  0.0
he_surf_s1(1)    =  2.0
```